Conclusions: The intra-observer variability in the diagnosis of prostate biopsies by WSI is the same as glass slide microscopy. Our results suggest that WSI could be used as an alternative to conventional microscopy for the first line diagnosis of prostate biopsies.

2168 Could Oligonucleotide Aptamer Probe Replace Antibody for Diagnosis?

Z Zeng, P Zhang, Y Zu. The Methodist Hospital, Houston, TX.

Background: Aptamers are small molecule ligands composed of short single-stranded oligonucleotides. The high sensitivity and specificity to their targets make aptamer an excellent candidate as a diagnostic probe. In addition, aptamer probes are easily generated through chemical synthesis. However, their potential clinical value has not yet been fully explored. In this study, we tested the aptamer probes for cell immunophenotyping, tissue immunohistochemical (IHC) stain, and blood circulating tumor cell detection.

Design: For immunophenotyping a CD30-specific aptamer was synthesized and conjugated with fluorochrome. Cultured lymphoma cells were stained with aptamer probe with antibodies and analyzed by flow cytometry. For IHC study the biotinylated aptamers were used. Formalin-fixed and paraffin-embedded lymphoma tissues were stained with aptamer probes and HRP-streptavidin reporter. For circulating tumor cell detection a novel assay system was developed by conjugating aptamer probe with both fluorochrome and quencher molecule. Normally, quencher molecule interacts with fluorochrome in the same aptamer sequence and renders it inactive.

Results: 1) Flow cytometry showed that the synthetic CD30 aptamer specifically stained anaplastic large cell lymphoma and Hodgkin lymphoma cells, but not control lymphoma cells that do not express CD30 [figure1A]. Cell staining patterns of aptamer probe were identical to CD30 antibody; **2)** Tissue IHC stains showed that aptamer probe specifically recognized CD30+ lymphoma cells, but did not react to background cells in tumor sites [figure1B]. The aptamer probe could efficiently stain tissues within shorter time than standard antibody; **3)** To detect circulating tumor cells a drop of blood from lymphoma patients was simply mixed with our new assay system, in which the aptamer-mediated cell binding and subsequent intracellular internalization resulted in endosomal degradation of aptamer sequence. Separation of fluorochrome from quencher molecule present in each aptamer probe activated fluorescent signals exclusively within lymphoma cells. This one-step assay could detect single tumor cell among thousands to millions of normal blood cells with no background [figure1C].

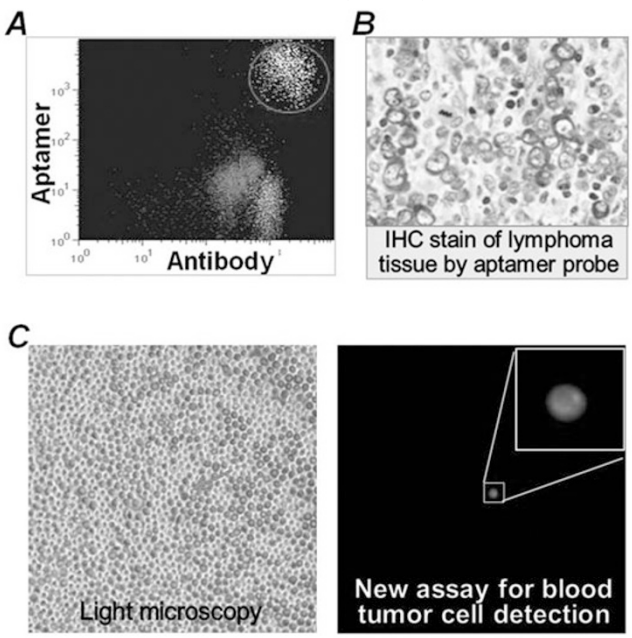

Conclusions: Our proof-of-concept studies demonstrated that the synthetic aptamer probe could replace antibody for disease diagnosis.

2169 Characteristics of Co-Amplification at Lower Denaturation Temperature-PCR (COLD-PCR) for *KRAS* Mutant Detection in Colorectal Carcinoma

S Zhang, J Tull. SUNY Upstate Medical University, Syracuse, NY.

Background: *KRAS* mutation analysis at codon 12 or 13 is important to predict response of targeted therapy against epidermal growth factor receptor (EGFR) on metastatic colorectal cancer with Erbitux. Clinical utility of regular PCR with Sanger's sequencing, a commonly used method, is limited by its low test sensitivity, i.e. 20% detection sensitivity of a mutant allele in a wild-type background. COLD-PCR provides a new approach of selective amplification on minority mutated alleles in a background of wild-type DNA. However, the characteristics of COLD-PCR plus Sanger's sequencing for *KRAS* mutation detection remains unclear in clinical samples of formalin fixed paraffin embedded tissue (FFPE).

Design: Eighteen FFPE samples of colorectal carcinoma with 10-80% tumor cellularity and known *KRAS* mutation were tested by regular PCR and COLD-PCR followed by Sanger's sequencing. The mutant to wild-type ratio between regular PCR and COLD-PCR were compared, and their correlation with tumor cellularity and variants of mutation were evaluated.

Results: The mutant/wild type ratios were generally increased in the group of COLD-PCR. However, the degree of increase was associated with mutant to wild-type ratio seen in regular PCR. When the ratios in regular PCR were ≤ 50% (8 cases), the ratios in COLD-PCR were increased by 82% on average. When the ratios in regular PCR were 50 ~ 130% (8 cases), the ratios in COLD-PCR were increased by only 19% on average. Interestingly, when the ratios in regular PCR were > 140% (2 cases), no increase or even reverse effect was observed in COLD-PCR group. Mutant/wild-type ratio was associated with tumor % cellularity only in a lower cellular group, and not related to types of *KRAS* mutation.

Conclusions: Improved *KRAS* mutant detection with COLD-PCR was demonstrated predominately in those with lower mutant/wild-type ratios, typically < 50%, in regular PCR. Through the COLD-PCR approach with Sanger's sequencing, test sensitivity for *KRAS* mutation can be elevated from 20% to 10% in general.

Ultrastructural

2170 Renal Disease with Underlying Mitochondrial DNA Mutations in Three Patients Lacking Electron Microscopic Mitochondrial Morphologic Abnormalities

LN Cossey, CP Larsen, HD Massey, TE Bunchman. University of Arkansas for Medical Sciences, Little Rock, AR; Nephropath, Little Rock, AR; Virginia Commonwealth University Medical Center, Richmond, VA.

Background: Congenital mitochondrial DNA (mtDNA) mutations are a rare cause of disease, and are often heralded by renal manifestations. Renal findings reported in association with mtDNA gene mutations vary, including nephromegaly and cyst formation grossly. By light microscopy, focal segmental glomerulosclerosis (FSGS), tubulointerstitial nephritis, and glomerular hilar hyaline lesions can be seen. And, by electron microscopy mitochondrial changes including increased numbers of mitochondria, binucleate forms, variations in size, shape and internal substructure disorganization and cristae loss are identified.

Design: Three renal biopsy specimens from patients with underlying mtDNA mutations were identified from Virginia Commonwealth University Medical Center. All biopsies were studied by light, immunofluorescence, and electron microscopy.

Results: All patients were Caucasian; two males (brothers, ages two and six) and one female (15 months). Two patients underwent percutaneous kidney biopsy, while one (s/p heart transplant) underwent autopsy. All patients were hypertensive with tubular and glomerular-based proteinuria. One patient had increased lactate levels, two patients had nephromegaly on ultrasound, and all had associated polyuria and polydipsia with normal renal function. Renal biopsies revealed focal segmental glomerulosclerosis in two patients and chronic tubulointerstitial injury/fibrosis in all patients. Electron microscopy showed intact glomerular basement membranes of appropriate thickness for age with no podocytopathy or immune complex deposits. Focal mitochondrial alterations (enlargement with substructure autolysis) consistent with fixation artifact were identified in one patient. In the remaining two patients no mitochondrial abnormalities were identified.

Conclusions: mtDNA mutations are a rare cause of renal disease and are largely undefined. In previous case series, striking electron microscopic mitochondrial and podocyte morphological changes have been associated with these mutations and described in up to 100% of study participants. Here, we have presented three mtDNA mutation patients with clinical and light microscopic changes consistent with those previously published but lacking the ultrastructural mitochondrial abnormalities which are classically described.

2171 Patterns of Proximal Tubulopathy in Monoclonal Light Chain-Associated Renal Damage Defined Ultrastructurally

GA Herrera, EA Turbat-Herrera. Nephrocor, Orlando.

Background: Proximal tubulopathy (PT) has been recognized as a pattern of renal damage in a subset of patients with circulating monoclonal light chains and renal manifestations. The clinical presentation may be sudden (acute renal failure) or slowly progressive renal dysfunction. Recognition of this entity requires careful immunomorphologic correlation.

Design: 3300 renal biopsies from 2 institutions over a period of 5 years were analyzed to identify cases of PT in patients with monoclonal light chain-associated renal dysfunction. Only those cases where the PT and related manifestations were the main pathologic findings associated with the renal damage were selected.

Specimen were examined by light, immunofluorescence, and electron microscopy with an emphasis on ultrastructural findings. Immunogold labeling, using a well described post-embedding protocol, was used in selected cases to correlate the localization of the monotypical light chains in specific compartments within the proximal tubular cells to highlight the pathologic findings.

Results: A total of 42 cases were found for a 1.6% incidence of this entity in this renal biopsy series. In all cases the proximal tubular damage was associated with monoclonal deposition of either κ or λ light chains in proximal tubules and surrounding interstitial compartment.

There were 4 distinct patterns of proximal tubular injury: 1- Tubular damage with features of acute tubular necrosis (apical blebbing, desquamation, fragmentation, vacuolization, and lysosomal proliferation in proximal tubular cells) (n=15), 2- Monotypical light chain deposition on the basolateral side associated with interstitial inflammatory response (n=21), 3- Intracytoplasmic crystalline-like inclusions in

proximal tubular cells (n=4), and 4- lysosomal accumulation with enlargement and atypical lysosomal forms ("lysosomal constipation" pattern) (n=2).
The most common patterns observed were 1 and 2. Pattern 3 was uncommon and only identified in 4 cases, while pattern 4 was the least common and only observed in 2 cases.
Conclusions: It is important to accurately identify the different patterns of PT in patients with monotypical light chain-associated renal damage. Ultrastructural evaluation together with immunofluorescence evaluation play crucial roles in confirming that the pathologic changes are indeed related to the pathologic circulating light chains. The findings by light microscopy may mimic a number of other unrelated pathologic processes. Ultrastructural labeling provides exquisite immuno-morphologic correlation in these cases and should be used in cases that require clarification.

2172 Role of Ultrastructural Evaluation of Peripheral Blood in Diagnosis of Metabolic Storage Disorders

J Hicks, E Wartchow, G Mierau. Texas Children's Hospital & Baylor College of Medicine, Houston, TX; Children's Hospital of Colorado, Aurora, CO.
Background: Lysosomal storage disorders in children are rare, occurring 1 in 1,500 to 7,000 births. These disorders are inherited deficiencies in 1 or more catabolic lysosomal enzymes. There are many steps necessary for synthesis and processing of lysosomal enzymes, making these processes prone to defects and dysfunction. Many different lysosomal storage disorders present in neonates, infants and young children with similar signs and symptoms.
Design: Surgical pathology and consultative archives of 2 pediatric hospitals were accessed over a 10 year period and identified 52 metabolic storage disorders that were diagnosed utilizing electron microscopy (EM) of peripheral blood mononuclear cells. Buffy coats comprised of peripheral mononuclear blood cells were prepared and examined by EM. The majority of the children were under 2 years of age (75%) with an age range from 1 month to 7 years.
Results: There were 3 categories of metabolic lysosomal disorders that were identified by characteristic storage material within peripheral blood mononuclear cells. Neuronal ceroid lipofuscinosis (Batten disease: mutations in CLN 1=>10 and CTSD genes) was most common(n=39/52) and the ultrastructural features allowed for characterization into infantile (granular osmophilic deposits), late infantile (curvilinear inclusions) and juvenile (fingerprint bodies) forms. Gaucher disease (β-glucocerebrosidase deficiency; n=9/52) was identified in the neonatal period (type 1) and early childhood (Type 3) with readily identified fine tubular helical/twisted structures distending the cytoplasm of mononuclear cells on ultrastructural examination. These tubular structures were seen in longitudinal and cross-sectional profiles and engorged the cytoplasm of peripheral blood mononuclear cells. Niemann-Pick disease (sphingomyelin-cholesterol lipidoses; sphingomyelinase deficiency) was identified in the remaining cases (n=4/52) in infants (Type A: infantile form). The inclusions in Niemann-Pick were characterized as pleomorphic lipid profiles that were generally membrane-bound whorled aggregates and multivesicular confluences with occasional lamellar material.
Conclusions: The current retrospective review demonstrates the utility of electron microscopy in evaluation of metabolic lysosomal storage disease in neonates, infants and children. Ultrastructural evaluation of peripheral blood mononuclear cells may provide for initial screening, preliminary diagnosis, and guide enzymatic and genetic testing.

2173 Effect of eNOS Deficiency on Glomerulonephritis in Murine Lupus-Like Model

J Hicks, T Schoeb, D Bullard. Texas Children's Hospital & Baylor College of Medicine, Houston, TX; University of Alabama - Birmingham, Birmingham, AL.
Background: Endothelial nitric oxide synthase (eNOS) is a constitutively active enzyme primarily expressed in endothelial cells and plays important roles in regulating vasodilatation, inhibiting smooth muscle proliferation and platelet aggregation, modulating leukocyte/endothelium adhesion events, and controlling key vascular functions. To examine the possible involvement of eNOS in the context of vasculitis and glomerulonephritis, *Nos3* (eNOS) mutation on background of MRL/MpJ-*Fas*^{lpr} mice (murine lupus-like model) was generated.
Design: MRL/MpJ-*Fas*^{lpr} mice deficient in eNOS were generated by sequentially backcrossing *Nos3* mutation (8 generations) onto MRL/MpJ-*Fas*^{lpr} strain, and homozygotes (*Nos3*$^{-/-}$) and heterozygotes (*Nos3*$^{+/-}$) were generated by intercrossing. Kidney tissues from eNOS+/+, eNOS+/-, and eNOS-/- genotyped MRL/MpJ-*Fas*^{lpr} mice were obtained for routine microscopic (H&E, PAS, trichrome) and electron microscopic examination. 5 mice in each of the 3 genotype groups were sacrificed at weeks 20 and 22.
Results: Wild type eNOS+/+ kidneys showed a moderate increase in mesangial cells and matrix without segmental lesions or crescents. There were readily identifiable intermediate to large electron dense deposits within the mesangium, paramesangium and basement membranes with foot process effacement. There were no vasculitic features and no deposits with the vessels or tubules. Heterozygote eNOS+/- kidneys showed a mild increase in mesangial cells and matrix with mesangial and paramesangial electron dense deposits. Frequency and size of deposits were decreased compared with eNOS+/+. Basement membrane deposits were not identified. There was no vasculitis or deposits with the vessels or tubules. Occasional aggregates of lymphocytes and plasma cells were present. Null eNOS-/- kidneys had mild mesangial matrix and cell increase. Mesangium and paramesangium contained fine small electron dense deposits. Rare small subendothelial deposits were seen. There were prominent perivascular aggregates of lymphocytes and plasma cells with electron dense deposits in perivascular adventitia.
Conclusions: eNOS deficiency in a murine lupus model tended to decrease mesangial, paramesangial and membranous deposits with its greatest effect in the null group (eNOS-/-). However, perivascular lymphoplasmacytic infiltrates with adventitial deposits occurred with the null eNOS-/- group. A partial loss of eNOS function may be beneficial in modulation of glomerulonephritis while avoiding vasculitis associated with complete loss of eNOS function.

2174 Neonatal Intrahepatic Cholestasis Associated with Citrin Deficiency (NICCD)

J Hicks, H-L Chen, Y Jeng, M-H Chang. Texas Children's Hospital & Baylor College of Medicine, Houston, TX; National Taiwan University Hospital, Taipei, Taiwan.
Background: Citrin, a mitochondrial inner membrane protein, functions as a calcium binding-stimulated aspartate-glutamate carrier component in nicotinamide adenine dinucleotide (NADH) shuttle. It is mainly expressed in the liver and participates in metabolic pathways (aerobic glycolysis, gluconeogenesis, urea cycle, protein/nucleotide synthesis). Citrin deficiency results in transient neonatal intrahepatic cholestasis (NICCD, recessive inheritance, Asian predilection). NICCD is characterized by prolonged cholestatic jaundice, low birthweight, growth retardation, hypoproteinemia, coagulopathy, anemia, hepatomegaly, liver dysfunction and hypoglycemia. Most undergo resolution by 1yr of age with appropriate treatment. Some have progressive liver disease requiring transplantation.
Design: Archives at National Taiwan University Hospital, following IRB, institutional and Department of Health approval, identified 9 neonates with genetically confirmed NICCD over a 16yr period. These neonates underwent liver biopsy and tissue was available for light and electron microscopic examination.
Results: NICCD liver biopsies showed variable degrees of cytoplasmic and canalicular cholestasis. Hepatocytes were arranged in pseudoacinar pattern. Diffuse microvesicular and macrovesicular steatosis involved vast majority of hepatocytes. Ballooning of hepatocytes was present; however apoptotic bodies were rare. Infrequent hepatocytes had undergone giant cell transformation. Occasional islands of extramedullary hematopoiesis were seen. The portal areas had mild increases in chronic inflammatory cells with no fibrosis and no bile duct proliferation. Central veins showed mild perivenule chronic inflammation. No viral cytopathic effect was seen. Electron microscopy showed hepatocytes with numerous lipid droplets of variable size. Some lipid droplets displaced and indented nuclei. Mitochondria tended to be small ovoid to slightly elongated with thick dense cristae, and not increased in numbers. Crystalline cristae were not seen. Intracytoplasmic bile was readily identified as dense aggregates. Typical peroxisome and glycogen particles were present. No viral inclusions were seen.
Conclusions: Neonatal intrahepatic cholestasis associated with citrin leads to marked lipid accumulation in hepatocytes with accumulation of intracytoplasmic bile profiles. NICCD in neonates and infants with jaundice should be a consideration in the differential diagnosis of cholestatic hepatitis with steatosis, especially in those with Asian descent.

2175 Preexisting Membranous Nephropathy in the Cadaveric Donor Kidney: Report of a Case

MK Mirza, K Henriksen, A Chang, SM Meehan. The University of Chicago Medical Center, Chicago, IL.
Background: Reports of transplanted donor primary glomerular immune complex mediated disease are uncommon. IgA nephropathy is the most commonly reported transplanted immune complex mediated disease with a frequency of 9-24% in donor biopsy specimens. Membranous nephropathy (MN) is rarely described with very few reports in the literature. The disease appears to resolve with little impact on graft function. We report a case of transplanted MN identified at the time of donor biopsy.
Design: Retrospective analysis of pathologic and clinical data of a case of transplanted MN was performed. Tissue sections were evaluated using H&E and PAS stains. Immunofluorescence microscopy was used to evaluate IgG, IgM, IgA, C3, C1q, fibrinogen and albumin. Electron microscopy was performed and Ehrenreich and Churg staging was used to assess lesions of MN.
Results: The donor was a 36 year old female with a history of hypertension, who died of a subarachnoid hemorrhage. She did not have detectable proteinuria. The recipient was a 61 year old male who underwent renal transplantation due to chronic renal failure (GFR 28 ml/min) and had concomitant heart transplantation due to long term diabetes mellitus complicated by severe coronary atherosclerosis and cardiac failure. Renal biopsy had never been performed. After transplantation, renal biopsies were obtained for increasing serum creatinine at days 17, 150, 225 and 825. PAS staining on all biopsies revealed basement membrane thickening with segmental 'spike' formation and vacuolization. Clinical and pathologic findings are summarized in Table 1.

Table 1.

	Pre-implantation	Day 17	Day 150	Day 225	Day 825
Cr (mg/dl)	N/A	1.9	1.7	1.3	1.4
Proteinurea	Nil	Nil	Trace	Nil	Trace
IF: IgG	3+	3+	3+	1-2+	trace - 1+
IF: C3	N/A	1-2+	1+	trace	trace
EM: Stage IV lesions	20-30%	40-50%	>90%	No EM	>95%
EM: Podocytes	FP preserved	FP preserved	FP preserved	No EM	FP preserved

IF: immunofluorescence microscopy, EM: electron microscopy, FP: Foot processes

Conclusions: Despite well developed lesions of MN, there was no correlation with podocyte foot process effacement or proteinuria in this patient. In the present instance there was a slow, but gradual resolution of lesions despite removal of the pathogenic environment. These observations suggest that a recipient environment that is non-immunogenic for MN, and perhaps immunosuppressive therapy, together facilitate resolution of immune complex deposits in transplanted MN.

2176 Alport-Like Changes in Allograft Glomerular Basement Membranes: A Peculiar Manifestation Occurring in a Setting of Pediatric Donor-Adult Recipient Renal Transplantation

MM Mishra, CMC Crisostomo, JR Lee, H Liapis, GA Youngberg. East Tennessee State University, Johnson City, TN; Mountain States Health Alliance, Johnson City, TN; Washington University School of Medicine, St. Louis, MO.
Background: We report a renal allograft with Alport-like electron microscopic (EM) changes and unique immunofluorescence (IF) findings. An adult with hypertensive nephropathy received an en-bloc transplant from a two year old male donor. The

clinical course was complicated by proteinuria (2.5g/24hrs), first detected 2.5 years post-transplant. Two renal biopsies were obtained, with the second showing unusual EM findings.

Design: The biopsy was examined using a standard protocol. Because of the EM findings, COL4A3 and COL4A5 stains were obtained.

Results: EM identified foci of multi-lamellation (basket-weaving) of the glomerular basement membranes (GBMs) simulating Alport syndrome (AS).

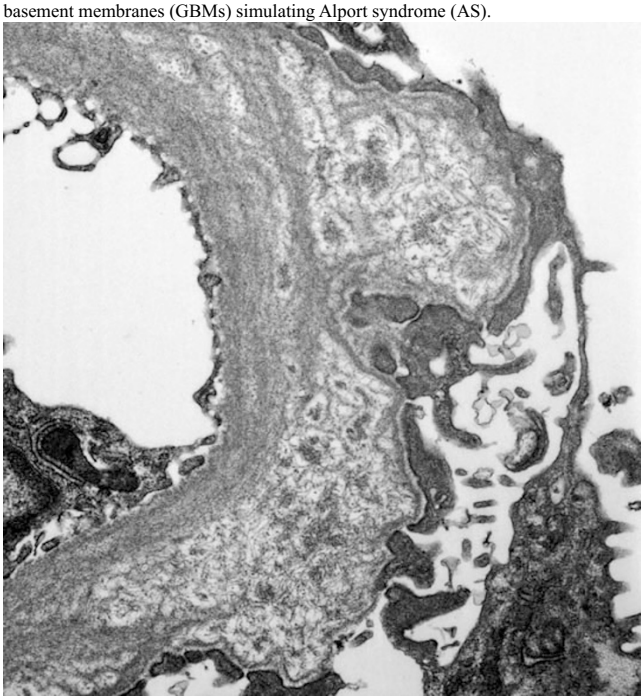

An IF study for COL4A3 and COL4A5 showed segmental loss of GBM staining; there was no history of AS in the donor or his family. The differential diagnosis included mechanical (perhaps hyperperfusion) injury in an immature kidney allograft from a young child to an adult. This unusual GBM injury may affect COL4 isoform staining due to degeneration of the lamina densa. This is the tenth case in the literature of AS-like GBM changes on EM in a post-transplant biopsy with no known history of AS in the donor. Eight of these cases involved pediatric-donor adult-recipient allografts. Our case is important in two aspects. It is the first reported case showing abnormalities on IF staining for COL4A3 and COL4A5 along with the AS-like EM changes. Only one of the previous cases had IF for COL4A3 and COL4A5, and the results showed no abnormality. Our case is only the second reported case involving a pediatric en-bloc kidney transplant into an adult (all the remaining reported cases involved pediatric-donor single kidney transplants).

Conclusions: This peculiar glomerular pathology is little recognized. It emphasizes the importance of EM in the evaluation of renal allograft biopsies and provides further evidence that en-bloc transplantation does not prevent the development of this clinically important post-transplant glomerular complication.